

Space Radiation Passive Dosimetry

Eric Benton

Radiation Physics Laboratory

Oklahoma State University

1. Introduction

Space radiation passive dosimetry consists of the use of passive radiation detectors to measure the dose and dose equivalent from ionizing radiation received during spaceflight and is one of the two main methods used to monitor the radiation exposure received by astronauts and cosmonauts. Passive space radiation dosimetry is commonly carried out with a combination of two types of detectors: 1) thermoluminescence detector (TLD) capable of measuring total absorbed dose, and 2) CR-39 plastic nuclear track detector (PNTD) capable of measuring the linear energy transfer (LET) spectrum, absorbed dose, and dose equivalent from charged particles of $LET_{\infty H_2O} \geq 5 \text{ keV}/\mu\text{m}$. Each crew member living and working aboard the International Space Station (ISS) wears a crew passive dosimeter (CPD) at all times consisting of these two types of radiation detector to provide the crew member's dose of record for the mission. Additional passive dosimeters are located at various positions throughout the habitable volume of the spacecraft. Following return to the ground, each passive dosimeter is processed and read out in the laboratory. The method and detectors are referred to as "passive" because they do not rely on active electronics or need electrical power for their operation and because, in general, they are incapable of providing time resolved data or data in real time.

2. Dosimeters for Space Radiation

2.1. Objectives of Space Radiation Dosimetry

The objectives of space radiation dosimetry include the following.

1. Accurately *monitor* the ionizing radiation exposure of space crews, permitting
 - 1.1. conduct of the mission so as to not exceed radiation limits;
 - 1.2. implementation of the ALARA (As Low As Reasonably Achievable) Principle.
2. Provide *warning* of potentially dangerous changes in the space radiation environment.
3. Document and provide an *archival* record of each crew member's radiation exposure history (i.e. dose of record). This information is used to:
 - 3.1. document that a crew member's career radiation limit has not been exceeded;
 - 3.2. inform astronauts of their risks from exposure to space radiation;
 - 3.3. provide data for ongoing and future epidemiological assessments of space flight radiation risks.
4. Provide information on the relative radiation exposures rates throughout the volume of the spacecraft and identify "hot spots" (i.e. areas of relatively high radiation flux) which ought to be avoided.
5. Provide important information related to the interpretation of instrument readings and experimental results.

It is in meeting the third objective that passive space radiation dosimetry is most useful.

2.2. Units of Measure

The fundamental quantity of radiation dosimetry is absorbed dose. Absorbed dose is the amount of energy absorbed per unit mass of a material when exposed to ionizing radiation:

$$D = \frac{E}{m}, \quad (1)$$

and is measured in SI units of joules/kg. Absorbed dose is typically cited in units of Gray (Gy) where 1 Gy = 1 Joule/kg. In many (often older) references, absorbed dose is cited in units of Rad, where 100 rad = 1 Gy.

Linear Energy Transfer (LET) is of central importance to space radiation dosimetry since it is this quantity that is measured by CR-39 PNTDs and Si spectrometers. LET is the amount of energy transferred by a energetic charged particle to the material through which is traveling per unit distance:

$$\text{LET} = \frac{dE}{dx} \quad (2)$$

In space radiation dosimetry, LET is typically given in units of keV/ μm (kiloelectron volts per micrometer). Absorbed dose can be determined based on knowledge of the fluence and the LET distribution of the incident radiation. For monoenergetic radiation:

$$D = \frac{1.602 \times 10^{-9} \Phi \cdot \text{LET}}{\rho} \quad (3)$$

where Φ is the fluence of particles, i.e. the number of particles per cm^2 , and ρ is the density of the material through which the particles are passing in units of g/cm^3 . The factor of 1.602×10^{-9} is needed to convert energy from units of keV to joules. The absorbed dose from a mixed radiation field (multiple types of particle) such as that encountered in space can be found by:

$$D = \frac{1.602 \times 10^{-9}}{\rho} \sum_i \Phi_i \cdot \text{LET}_i \quad (4)$$

where Φ_i is the fluence of particles having LET_i .

Early in the history of research on the biological effects of ionizing radiation, it was found that identical doses of different types of radiation produced different amounts of damage to biological systems. For example, the damage produced in an a laboratory animal exposed to 1 Gy of α -particles was more severe than the damage produced by a 1 Gy exposure of γ -rays. This observation gave rise to the concept of dose equivalent. The dose equivalent is equal to the absorbed dose multiplied by a unitless weighting or quality factor which takes into account the fact that ability of radiation to inflict biological damage depends on the LET of the radiation:

$$H(\text{LET}) = D(\text{LET}) \cdot Q(\text{LET}). \quad (5)$$

The LET-dependent quality factor is defined:

$$Q(\text{LET}) = \begin{cases} 1.0 & \text{LET} < 10 \\ 0.32 \cdot \text{LET} - 2.2 & 10 \leq \text{LET} \leq 100 \\ 300 / \sqrt{\text{LET}} & \text{LET} > 100 \end{cases} \quad (6)$$

where LET is in units of keV/μm [ICRP, 1991].

2.3. Radiation Exposure Limits for Space Crew

The National Council on Radiation Protection and Measurement (NCRP) has made recommendations for the exposure of astronauts in LEO. The exposure limits currently in use by NASA for LEO were published in NCRP Report No. 132 in 2000 [NCRP, 2000]. The 10 year whole-body radiation exposure limits based on a 3% excess lifetime risk of fatal cancer as recommended by the NCRP are shown in Table 2.1. The organ-specific radiation exposure limits for deterministic (non-stochastic) effects as recommended by the NCRP 2000 report are shown in Table 2.2. It should be noted that the recommended limits are only for astronauts living and working in LEO. No recommendations have yet been made for deep space exploration missions such as a return to the moon or a trip to Mars.

Table 2.1. Ten year career whole-body limits based on 3% excess lifetime risk of cancer mortality as recommended in NCRP Report 132 [NCRP, 2000].

Age	NCRP-132 Equivalent Dose (cSv)	
	Female	Male
25	40	70
35	60	100
45	90	150
55	170	300

Table 2.2. Non-stochastic organ dose/dose equivalent limits for all ages and both genders as recommended in NCRP Report 132 [NCRP, 2000].

	NCRP-132 Gray Equivalent (cGy)		
	BFO*	Eye	Skin
Career	—	400	600
Annual	50	200	300
30 days	25	100	150

*Blood Forming Organ

2.4. Constraints

Due to the complexity of the space radiation environment in LEO, the accurate measurement of astronaut and cosmonaut exposure to ionizing radiation during spaceflight may well represent the single most difficult challenge in dosimetry for radiation protection. The composition of the radiation environment in LEO, coupled with a requirement for compact, light-weight and autonomous instrumentation for use aboard spacecraft, mean that ordinary, off-the-shelf dosimeters cannot be used and that specialized instrumentation and methods must be employed.

An instrument to be used for dosimetry aboard spacecraft should possess a number of features and properties. Due to space constraints aboard spacecraft, it is important for the dosimeter to be compact, light-weight, and unobtrusive. In the case of personal dosimeters, it is crucial that the device not interfere with the normal working routine of astronauts and that its operation requires only a minimum of user intervention. The dosimeter needs to be robust and capable of operating under a variety of different conditions. The device ought to be fairly inexpensive to purchase, operate, and, if necessary, readout and analyze. Finally, it is desirable that the detector(s) used in the dosimeter be tissue equivalent or nearly tissue equivalent so as to readily relate measured dosimetric quantities to potential effects in humans.

Naturally it is necessary for the dosimeter to be sensitive to the major ionizing radiation components at the relevant energies present in a given environment. A dosimeter for use aboard manned spacecraft should be sensitive to both the primary particles of the galactic cosmic ray (GCR), solar particle, and trapped particle components, and to secondaries produced when primary particles interact with the mass of the spacecraft and its contents, including the bodies of the astronauts (see Section 3).

The first decision to be made when choosing the type of detector(s) to be used in a dosimeter is whether to use active or passive detectors. The major advantages of active detectors are that they provide time resolved data and can be read out in real time. However, active detectors tend to be significantly larger and more massive than their passive counterparts, and they require a constant source of power. In the case of a personal dosimeter, this power source usually takes the form of a battery, adding additional mass and volume to the instrument. Passive detectors, in addition to being lighter and more compact than active detectors, are less likely to undergo mechanical or electronic failure and are immune to power interruptions. The major disadvantage of passive detectors is that they can only measure a total, cumulative signal and cannot resolve any time dependence in the signal. Processing and readout of passive detectors can also be quite involved and usually needs to be carried out in a ground-based laboratory after completion of the mission.

The advantages inherent in passive detectors—small size, low mass, safety, relative ease of use and zero power consumption—have made them the detector of choice for much of the history of human spaceflight. Passive detectors have most commonly been used for crew dosimetry and just about every astronaut and cosmonaut who has flown in space has carried at least one passive dosimeter. Passive detectors used for crew and area dosimetry aboard piloted spacecraft have been mainly of two types: thermoluminescence detectors (TLDs) and solid state nuclear track detectors (SSNTDs). The type of TLD most widely used is lithium fluoride (LiF), although other types of thermoluminescence material have also been employed. Among the disadvantages of

TLDs is that they provide no LET information and consequently no information about the dose equivalent. In addition TLDs tend to record the dose for high LET (≥ 10 keV/ μm) radiation with less than 100% efficiency—thus, systematically undermeasure the total dose [Benton et al., 2000]—and are relatively insensitive to neutrons [Benton et al., 2001]. Of the various types of SSNTD, those made of organic polymers, most notably CR-39, are the most sensitive. CR-39 plastic nuclear track detector (PNTD) has a sensitivity threshold to charged particles of $\text{LET}_{\infty\text{H}_2\text{O}}$ equal to ~ 5 keV/ μm .

Numerous research groups have developed techniques for combining absorbed dose measurements from TLDs with the LET spectrum measured in CR-39 PNTDs, yielding total dose equivalent [Doke et al., 1984; Benton et al., 2002]. Absorbed dose is measured using LiF TLD while CR-39 PNTDs are used to measure the $\text{LET}_{\infty\text{H}_2\text{O}}$ spectrum ≥ 10 keV/ μm . The high LET contribution to total dose measured by the PNTDs is subtracted from the TLD absorbed dose with the aid of an empirically determined dose efficiency function [Benton et al., 2000]. The remaining TLD dose is assumed to have a quality factor of 1 and is combined with the dose and dose equivalent spectra measured by the PNTDs to yield corrected total dose, dose equivalent and mean quality factor. This method has seen widespread application aboard US and Russian spacecraft and recoverable satellites over the last three decades.

A principal disadvantage of passive detectors is their inability to provide real time or time-resolved data. The Pille TLD System, developed by the KFKI Atomic Energy Institute, Budapest, partially overcomes these limitations [Apathy et al., 1999]. The Pille System permits TLDs to be read out, annealed, and re-used on orbit. In one form or another, the Pille system has been in use aboard Russian spacecraft since the Salyut-7 Orbital Station missions and two units are installed aboard the ISS.

There are other different types of passive detectors including photographic nuclear emulsions, activation foils and fission foils. Photographic nuclear emulsions are considerably more sensitive than SSNTDs. However, they are too difficult to handle and analyze to be suitable for use in routine space crew dosimetry. In the first decades of human spaceflight, before the development of CR-39 PNTD, other types of PNTD such as Cellulose Nitrate (CN) and Lexan Polycarbonate were widely used and are still used for specialized applications.

3. Space Radiation Environment

Astronauts and experimental payloads aboard low-Earth orbit (LEO) spacecraft like the Space Shuttle and ISS are exposed to levels of ionizing radiation far in excess of that encountered on the ground. Charged particles in the form of galactic cosmic rays (GCR), trapped protons and electrons, and particles emitted by the sun during solar flares and coronal mass ejections constantly impinge on the outer surface of the spacecraft. The more energetic of these particles penetrate the skin of the spacecraft, interacting with the mass of the spacecraft and its contents, including the bodies of the astronauts, therein depositing energy that can potentially result to damage to living cells. Energetic primary particles can also undergo nuclear interactions with the mass of the spacecraft and its contents, producing energetic secondary particles in the process. Secondary particles, especially high energy neutrons, can possess a greater radiobiological effectiveness than the primary particles which produced them. Because of the different types of

radiation found in LEO and the broad energy range they occupy, dosimetry aboard spacecraft like the ISS is significantly more challenging than on the ground.

3.1. Galactic Cosmic Rays

Galactic cosmic rays (GCR) are energetic charged particles that originate from sources beyond our solar system. The distribution of GCR is thought to be isotropic throughout interstellar space. The energies of GCR particles range from several tens of MeV up to 10^{20} eV and occupy a broad peak centered at about 1 GeV/nucleon. The GCR spectrum consists of 98% protons and heavier ions (baryon component) and 2% electrons and positrons (lepton component). The baryon component is composed of 87% protons, 12% helium ions (alpha particles) and 1% heavy ions of charge 3 (Li) through 92 (U). Iron plays a particularly important role in space dosimetry because it is both high in LET and is relatively plentiful compared to other high Z ions [NCRP, 1989].

The flux of GCR in the solar system is affected by the sun's eleven year cycle. During that period of the solar cycle called Solar Maximum, when solar activity is most intense, the solar wind attenuates a greater flux of the inbound GCR than during Solar Minimum, when solar activity is least intense. During Solar Minimum, the maximum flux of GCR is able to penetrate into the inner solar system.

GCR, being composed of charged particles, is also affected by the Earth's magnetic field. Charged particles tend to follow the lines of the geomagnetic field. Since the geomagnetic field lines are parallel to the Earth's surface above the equator, most of the particles are deflected away and only very high energetic particles reach LEO. The geomagnetic field over the North and South Poles is oriented perpendicular the Earth's surface and GCR particles of all energies are funneled toward the poles at high latitudes. The 51.56° orbit of the ISS is sufficiently highly inclined to receive a substantial exposure from less energetic GCR [Benton and Benton, 2001].

3.2 Trapped Particles

Surrounding the Earth are intense regions or "belts" of trapped protons and electrons. Protons and electrons are trapped by the geomagnetic field where they spiral around the magnetic field lines, bouncing back and forth from mirror points near the magnetic poles. The trapped electron spectrum extends in energy from tens of keV to ~6 MeV. Trapped protons extend in energy from several MeV to several hundred MeV and possess a broad peak around 100 MeV. Because the electrons are of low energy they are stopped by the shielding provided by the skin of the spacecraft and present little risk to space crew. Only the most energetic electrons, interacting with the mass of a spacecraft and its contents, will produce Bremsstrahlung X-rays [Stassinopolus, 1988].

The majority of the trapped proton belt lies at altitudes above that traversed by the orbit of the ISS. However due to the fact the axis of the Earth's magnetic field is slightly displaced from the Earth's axis of rotation, there is a region off the coast of Brazil called the South Atlantic Anomaly (SAA) where the geomagnetic field drops unusually close to the Earth's surface and

the trapped proton belt intersects the orbits of low altitude spacecraft such as the Space Shuttle and ISS. When the ISS passes through the SAA, it receives its maximum exposure to trapped protons. For the 51.56° inclination, ~400 km altitude orbit of the ISS, about half the ionizing radiation dose is from trapped protons in the SAA and half is from GCR at higher latitudes [Benton and Benton, 2001].

3.3 Solar Particle Events

The third source of ionizing radiation in LEO is from energetic particles emitted from the sun during solar flares and coronal mass ejections. These solar particle events (SPE) are relatively rare and occur most often during the Solar Maximum phase of the eleven year solar cycle. Most SPEs consist primarily of low energy protons, although higher energy protons and heavy ions can also be emitted. Warning of SPE is often possible ahead of time (a solar flare is seen in the visible light and radio spectra before the SPE arrives at the Earth) allowing astronauts and cosmonauts time to return inside the spacecraft during EVA and remain in the most heavily shielded portion of the spacecraft until the event is over [Reames, 1999].

Like charged particles from the other space radiation sources, the particles emitted by the sun during an SPE are affected by the Earth's magnetic field. SPE exposure of the ISS only occurs when the station is near the magnetic poles.

3.4 Secondary Particles

As charged particles pass through matter, they interact with the matter in one of two ways: 1) through ionization or 2) through nuclear interactions. Ionization occurs when an incident charged particle interacts with the electrons of the matter through which it is traveling. Some of these electrons are stripped away from their constituent atoms, leaving the atoms in a highly reactive, ionized state. A nuclear interaction occurs when a charged particle collides with the nucleus of an atom in the material through which it is passing. Such nuclear interactions can produce secondary particles including neutrons and recoil nuclei. A second source of lower energy neutrons are the albedo neutrons, produced by nuclear interactions of GCR with the nuclei in the Earth's atmosphere. Neutrons are uncharged, so they do not interact with matter via ionization. Instead they are very penetrating and readily interact with atomic nuclei via the nuclear strong force.

One way in which ionizing radiation is quantified is in terms of Linear Energy Transfer (LET) spectra. The LET of a particle is a measure of the change in the energy of the particle per unit path length (distance) in the material through which it is traveling (e.g. water or human tissue) and varies inversely with the kinetic energy of the particle. A particle's LET is believed to be of greater relevance than its total kinetic energy in terms of radiobiological significance, since LET is a measure of the energy actually transferred to the surrounding medium through which the particle passes. This transferred energy results in ionization of the surrounding matter and is responsible for biological damage if the particle is passing through tissue. It is through ionization that the chemical changes in tissue occur that lead to mutations and other stochastic effects.

Interactions between secondary neutrons and the nuclei of the surrounding medium often result in high LET particles possessing a large radiobiological effectiveness. Charged particle secondaries in the form of projectile and target fragments ejected in collisions between primary charged particles and the nuclei of the spacecraft often possess a higher LET than the original primary particle and consequently may also possess a greater radiobiological effectiveness.

4. Thermoluminescence Detectors

Thermoluminescence detectors (TLDs) are the most commonly used radiation detector in space radiation dosimetry and are used to measure absorbed dose from all forms of ionizing radiation. TLD is a type of detector belonging to a group known as luminescence detectors. Other types of luminescence detectors used in space radiation dosimetry are optically stimulated luminescence detectors (OSLDs) and silver metaphosphate glass detectors.

Luminescence detectors take the form of dielectric crystalline materials such as LiF, CaSO₄, or Al₂O₃ that are doped with minute quantities of impurity atoms during the crystal growth process. Figure 4.1 shows a band gap diagram that illustrates the operation of TLD and OSLD. Electrons of the crystal that are tightly bound to individual atoms are said to be in the valence band, while electrons shared amongst the many atoms of the crystal are said to be in the conduction band. The impurity atoms in the crystal serve as electron and hole traps in the forbidden gap between the valence and conduction bands. In dielectric crystalline materials such as those used for TLDs and OSLDs, the conduction band is usually empty and all the electrons in the crystal are found in the valence band.

As shown in Figure 4.1 (a), the passage of a charged particle through the detector elevates electrons into the conduction band, leaving holes in the valence band and thereby creating electron-hole pairs. Similarly, absorption or scattering of a high energy photons (γ - or x-rays) by valence band electrons can create electron hole pairs. Ordinarily these electron hole pairs quickly recombine. However, in a luminescence material such as a TLD, when electrons and holes try to recombine, they can become trapped in the sites within the forbidden gap created by the presence of the impurities. Recombination is then impossible without the introduction of a small amount of energy to elevate the electrons and holes out of their respective traps. In TLD, this extra energy takes the form of heat, while in OSLD, this energy takes the form of visible light from a laser as shown in Figure 4.1 (b). During the recombination process, the excess energy of the electrons moving from the higher energy state of the trap within the forbidden gap to the lower energy ground state of the valence band is given off in the form of photons of visible light. This light can be amplified and its intensity measured with the aid of a photomultiplier tube. The amount of light emitted as a result of recombination of electrons with the valence band is proportional to the amount of energy deposited by the original energetic charged particle or photon of radiation and thus proportional to the absorbed dose deposited by the passage of a charged particle through the crystal.

Because the TLD only emits light when it is heated, there is no way to know when or for how long the TLD was exposed to radiation. Thus it is only possible to obtain dose rate information averaged over the duration of the TLD exposure. In addition, there is no way to tell anything

about the total kinetic energy or the charge of the incident radiation responsible for the dose measured in the TLD. OSLD and silver metaphosphate glass detectors have similar limitations.

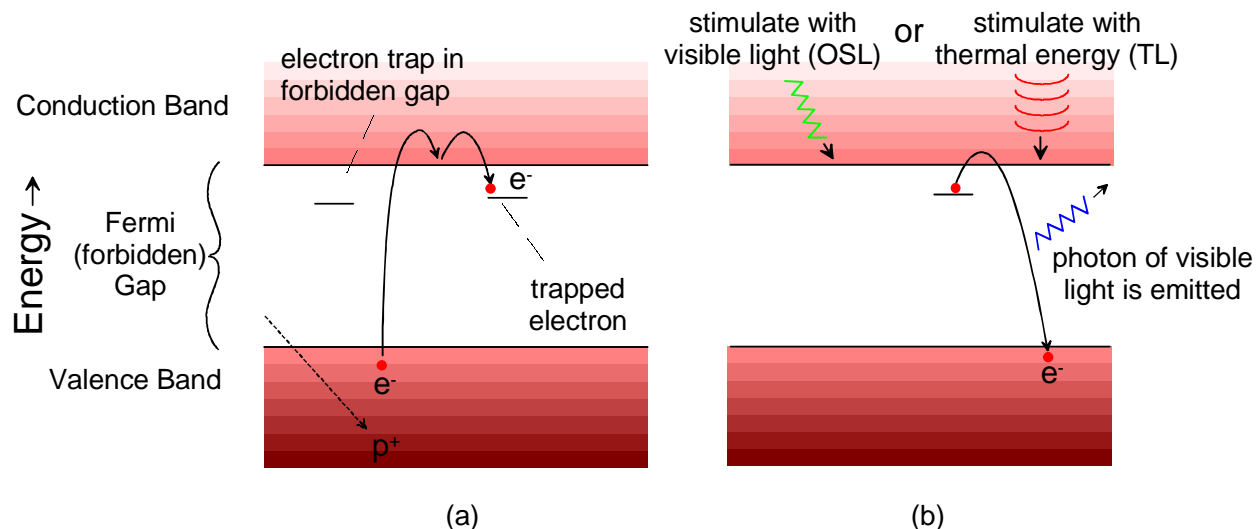


Figure 4.1 Thermoluminescence and optically stimulated luminescence mechanisms illustrated by means of a band gap diagram.

TLDs are analyzed through use of a dedicated TLD reader which contains of a light-tight cavity, a planchet on which the TLD is heated, and a photomultiplier tube to measure the light output from the TLD during heating. The reader heats the TLD using a preset heating profile specifying temperature (in terms of the electrical current used to heat the planchet) as a function of time. The electronics of the reader then record the light output of the TLD as measured by the photomultiplier tube as a function of temperature and converts this to a digital signal using an analog to digital converter (ADC). The result is a “glow curve.” An example of a glow curve for a CaSO₄:Dy TLD exposed to ~2 mGy ¹³⁷Cs γ -rays and read out using the Pille TLD system is shown in Figure 4.2. The integrated area under the glow curve is proportional to the absorbed dose received by the TLD over the course of the exposure.

By reading out a large number of TLDs exposed to known doses of radiation, the TLD material can be calibrated and a mathematical function relating TLD light output to absorbed dose is obtained. When a TLD exposed to an unknown dose of radiation is read out, its light output is converted to total dose using this function. This type of calibration applies only to a given manufactured batch of TLD material that is read out using the same heating profile. During field measurements, several TLDs are often exposed together and the average TLD dose reading is obtained.

The TLD method of radiation dose measurement possesses a number of limitations. One of these is the decreased efficiency with which it is able to record the dose from high- LET radiation [Benton et al., 2000]. When a heavy ion traverses a TLD, the density of traps immediately surrounding the particle’s trajectory is not sufficient to trap all the energized electrons and the electron traps quickly become saturated. Thus some of the dose deposited by the heavy ion is not

stored as trapped signal and the dose read out from the TLD will be systematically low. To compensate for the reduced dose registration efficiency at high-LET, an empirical dose efficiency function is measured based on high-LET heavy ion exposures at ground-based accelerators.

Table 4.1 shows a representative sample of absorbed doses and average dose rates measured using TLDs aboard a variety of different spacecraft and aircraft. The NASA ER-2 is a high altitude research aircraft similar to the U-2 spy plane. Generally speaking, average dose rate scales with altitude. The highest dose rates are for high altitude, low orbital inclination flights of the Space Shuttle that receive substantial dose from trapped protons encountered in the South Atlantic Anomaly.

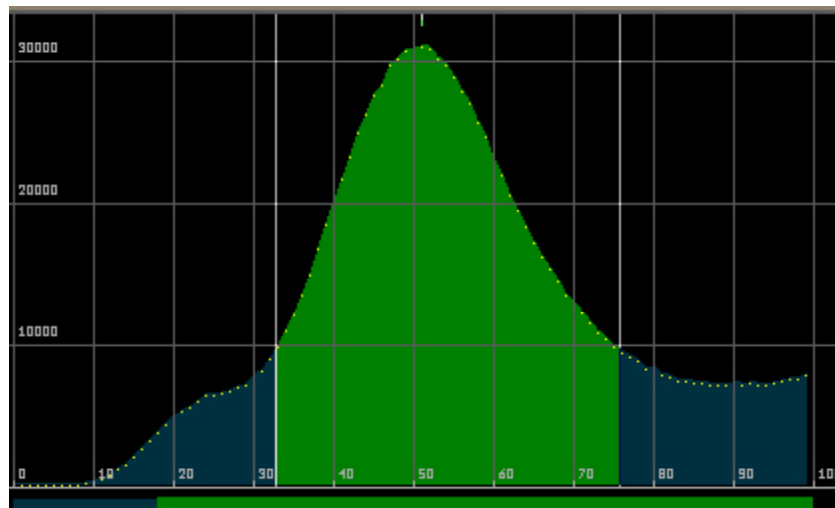


Figure 4.2 Glow curve measured using the Pille TLD system. The x axis is in units of channel number of the ADC and is proportional to planchet temperature (heating current). The y axis is in relative units of light intensity. The integrated area of the highlighted peak region gives the dose by means of the calibrated detector response function.

Table 4.1. Representative sample of absorbed doses and average dose rates measured using TLDs aboard a variety of spacecraft and aircraft.

Exposure	Dates	Duration (hr)	Average Altitude (km)	Orbital Inclination	Absorbed Dose (mGy)	Average Dose Rate (μ Gy/hr)
Apollo 11	7/1969	194	Lunar Mission		1.8	9.2
Apollo 14	1/1971	216	Lunar Mission		11.4	52.9
STS-57 Space Shuttle	6/21/1993	240	462	28.5°	9.2 \pm 2.1	38.5 \pm 8.9
STS-60 Space Shuttle	2/3/1994	199	352	57°	1.4 \pm 0.4	6.9 \pm 1.9
ISS Expedition 2 (low shielding)	5-8/2001	2350	400	51.56°	17.5 \pm 1.6	7.5 \pm 0.7
ISS Expedition 2 (high shielding)	5-8/2001	2350	400	51.56°	23.8 \pm 1.9	10.1 \pm 0.8
Commercial 747 Dublin/LA route	8-10/2001	796	10	na	2.0 \pm 0.1	2.5 \pm 0.2
NASA ER-2 >60° N. lat.	1-6/2000	46.5	20	na	0.4 \pm 0.1	8.4 \pm 1.3
NASA ER-2 ~34° N. lat.	6-10/2002	65.2	20	na	0.2 \pm 0.1	2.4 \pm 0.6
TRACER Antarctic Balloon	12/2003	324	37.5	na	1.6 \pm 0.1	4.9 \pm 0.2

5. CR-39 Plastic Nuclear Track Detector

CR-39 (polyallyldiglycol carbonate) is a crosslinked thermoset polymer having the chemical formula $C_{12}H_{18}O_7$. Since its initial use as a nuclear track detector in 1978 [Cartwright et al., 1978; Cassou & Benton, 1978], CR-39 has remained the most radiation-sensitive PNTD in common use and can register tracks from charged particles of $LET_{\infty}H_2O$ between ~ 5 and ~ 1500 keV/ μm . CR-39 is sensitive to protons of energy ≤ 10 MeV, α -particles of energy ≤ 50 MeV/n, and heavy ions of all energies. Neutrons of energy between 1 and 20 MeV are detected via tracks from recoil protons formed in interactions between incident neutrons and the hydrogen of the CR-39 PNTD. Higher energy protons and neutrons are detected via target fragmentation reactions with the C and O nuclei of the PNTD or in target materials immediately adjacent to the detector. In space dosimetry, CR-39 PNTD is used to measure the LET spectrum, absorbed dose, and dose equivalent from primary and secondary charged particles of $LET \geq 10$ keV/ μm . In form, a CR-39 PNTD is a thin (~ 0.6 mm) layer of transparent plastic.

When a charged particle possessing an LET in excess of the minimum threshold for track registration passes through a layer of CR-39 PNTD, it breaks many of the molecular bonds of the polymer in the region immediately surrounding its path. The result is that a trail of highly chemically reactive sites is created along the particle's trajectory. This path through the bulk of the detector is referred to as a "latent damage trail." Following exposure and return of the PNTD to the laboratory, it is chemically processed or "etched" in a strongly alkaline solution (e.g. 6.25 N NaOH at 50°C) for a predetermined length of time. The alkaline solution attacks and dissolves away the bulk of the detector at an angle perpendicular to any exposed surface at a rate V_G , referred to as the bulk etch rate. However it attacks and dissolves away the latent damage trail along the particle trajectory at a rate V_T , referred to as the track etch rate, that is greater than the bulk etch rate. This results in a conical pit forming at the site of the latent damage trail which can be viewed under an optical microscope following etching. Both V_G and V_T are typically quoted in units of $\mu m/hr$. The size of the elliptical opening of the conical etch pit is proportional to the LET of the particle that produced the original latent damage trail. Figure 5.1 shows the evolution of a nuclear track through chemical etching.

The bulk etch rate, V_G , is a property universal to the detector material and the given etch conditions (etchant composition, concentration, temperature, etc.). The track etch rate, V_T , is dependent on these factors as well as on the rate of energy deposition (LET) of the incident charged particle as it traversed the detector and produced the latent damage trail. The ratio of V_T to V_G is referred to as the reduced etch rate ratio, V_R [Henke & Benton, 1971]:

$$V_R = \frac{V_T}{V_G}. \quad (7)$$

In order for a latent damage trail to be transformed by chemical etching into a conical nuclear track, V_R must be greater than 1. The angle between the axis of the track (congruent to the latent damage trail and the trajectory of the of the charged particle) and the sides of the conical track is referred to as the cone angle θ . The sine of θ is equal to the reciprocal of V_R :

$$\sin \theta = \frac{1}{V_R} = \frac{V_G}{V_T}. \quad (8)$$

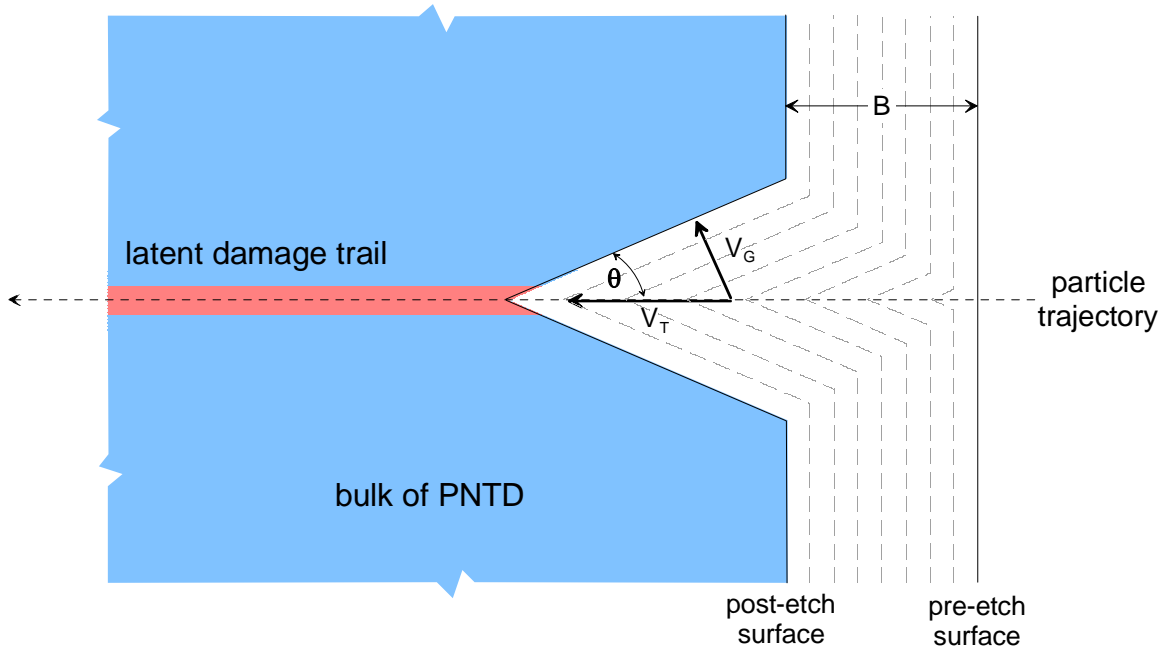


Figure 5.1. Formation of a visible nuclear track in PNTD through chemical etching.

It is the quantity V_R is of principal interest when measuring a nuclear track since it is proportional to 1) the LET of the charged particle in the region of the detector where the latent damage trail was formed, and 2) to the size of the elliptical intersection of the conical track with the post-etch surface of the detector. Particles of greater stopping power displace a larger number of electrons, breaking a greater number of chemical bonds, and hence produce latent damage trails that are more reactive to the chemical etchant. Cone angle, θ , is inversely proportional to the stopping power. A particle of low stopping power produces a larger θ and a shallower track than does a particle of higher stopping power. In a PNTD layer that has been etched to remove a thickness B of detector material (bulk etch), the value of V_R for a track can be found by:

$$V_R = \sqrt{1 + \frac{4\left(\frac{a}{B}\right)^2}{\left[1 - \left(\frac{b}{B}\right)^2\right]^2}}, \quad (9)$$

where a and b are the dimensions of the semi-major and semi-minor axes, respectively, of the elliptical opening of the track (intersection of the conical track with the post-etch surface of the detector) as illustrated in Figure 5.2.

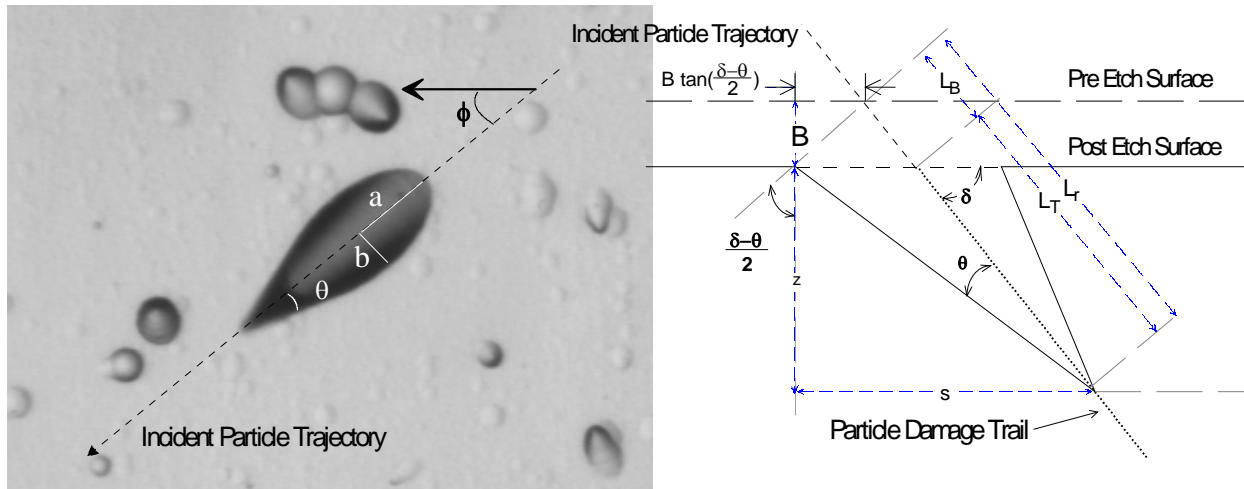


Figure 5.2. Geometry of a typical track in CR-39 PNTD.

In accelerator experiments, CR-39 PNTDs can be exposed normal (90°) relative to the incident particle beam. This results in circular tracks that are easy to measure. Figure 5.3 shows tracks from particles of varying stopping power in CR-39 PNTD exposed for calibration purposes at the HIMAC heavy ion accelerator in Japan. In accelerator exposures the energy and Z of each track are known since we can measure them independently at the accelerator. The same cannot be said for detectors exposed in space. Here the particles penetrate the detector at all angles, giving rise to tracks of varying eccentricity. Figure 5.4 shows tracks in a layer of CR-39 PNTD exposed aboard the ISS. It is sometimes possible to see the results of nuclear interactions in CR-39 PNTD. Figure 5.5 shows tracks from secondary particles produced in CR-39 PNTD exposed aboard the NASA ER-2 high altitude research aircraft (civilian version of the U-2 spy plane) at $\sim 70,000$ ft (~ 20 km). A high energy neutron or proton collided with a heavy nucleus just above the detector layer (probably part of the protective covering over the CR-39 PNTD). This heavy nucleus then disintegrated into (at least) three short range, high LET secondary particles which formed tracks in the CR-39 PNTD.

The readout of a layer of CR-39 PNTD consists of locating all the tracks within a given area on the detector's surface and measuring the size of their semi-major and semi-minor axes. This is done using a standard optical microscope at a magnification of between about $100\times$ to $500\times$. The value of V_R is calculated for each measured track. Then the LET of that track is determined based on an empirical detector response or calibration function which directly relates LET to V_R . After that, the LET data for all the tracks measured totaled up and normalized to the area measured on the detector surface. The result is an LET spectrum.

Table 5.1 shows the average absorbed dose rate, average absorbed dose equivalent rate and average quality factor (ratio of dose equivalent to dose) for particles of $LET \geq 10$ keV/ μm measured aboard these spacecraft and aircraft. Figure 5.6 shows the average integral LET flux spectra measured on the ISS, aboard a commercial jetliner flying at an average altitude of 10 km between Dublin, Ireland and Los Angeles, on a NASA ER-2 high altitude research aircraft flying at an average altitude of 20 km and above 60° North Latitude, and for an Antarctic balloon

mission flying at an average altitude of 37 km. Each spectrum is read right to left with each point on a curve representing the number of particles per square centimeter, steradian (unit solid angle), hour having LET greater than or equal to the corresponding value on the x -axis. Thus the total flux of particles having LET ≥ 5 keV/ μm per $\text{cm}^2\cdot\text{sr}\cdot\text{hr}$ is represented by the left-most point on each curve.

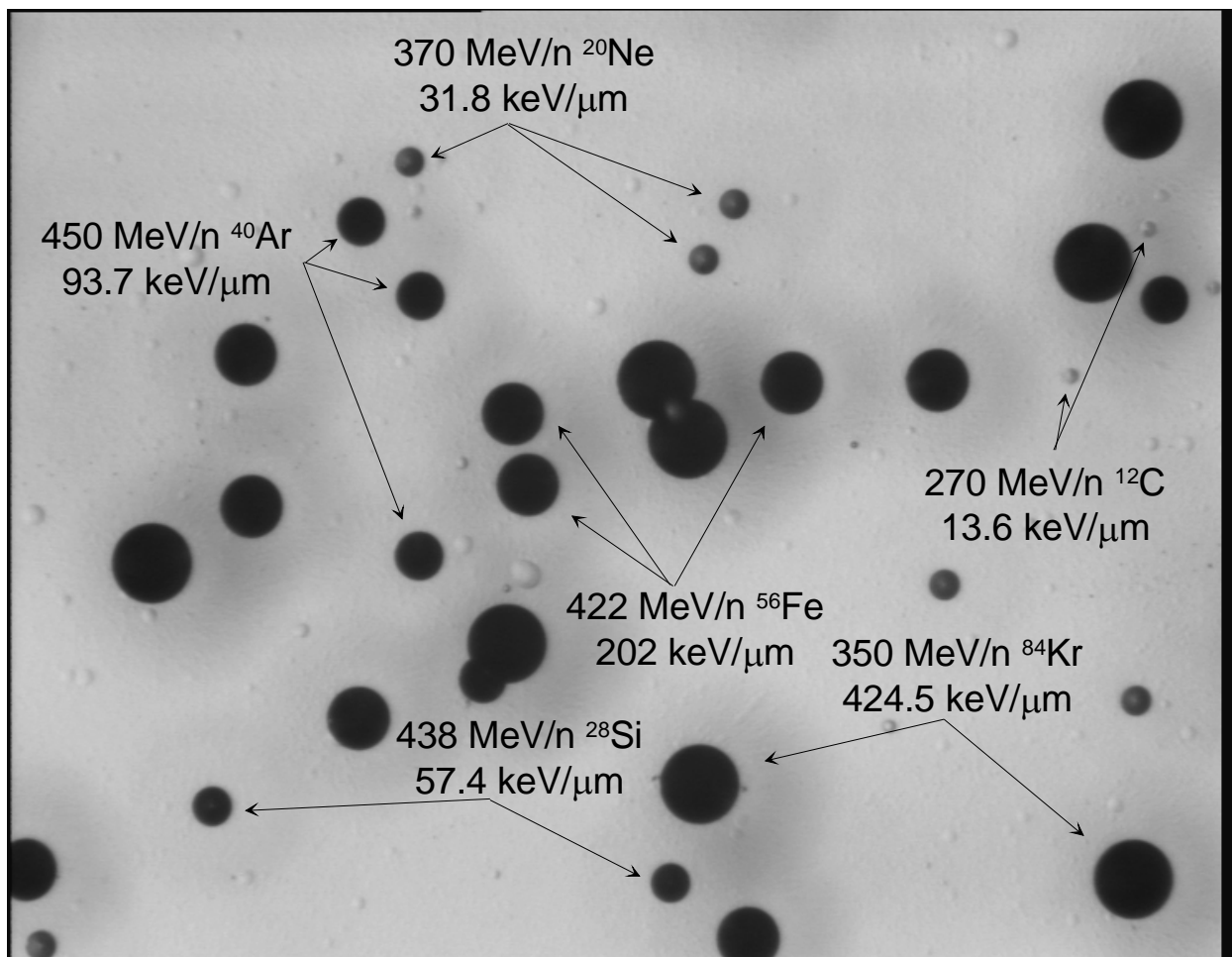


Figure 5.3. Heavy ion tracks of different stopping power in CR-39 PNTD.

Not surprisingly, the lowest flux is measured aboard the commercial jetliner at the lowest altitude and deep within the Earth's atmosphere, followed by the ER-2 high altitude research aircraft. The majority of the tracks in CR-39 PNTDs exposed aboard the commercial jetliner and ER-2 are from secondary protons and heavy ions produced inside the detector following collisions with energetic neutrons in the atmosphere. The spectrum measured aboard the Antarctic balloon lies for the most part above that measured aboard the ISS despite the fact that the altitude of the ISS (~400 km) is well above that of the balloon (~37 km). The reason for the higher flux of the Antarctic balloon comes from the fact that near the Earth's magnetic poles, the geomagnetic field provides little or no shielding from GCR, while at lower latitudes, even while at higher altitudes, the geomagnetic field deflects away a substantial fraction of the GCR. Of

course the ISS measurement contains a contribution from trapped protons and trapped proton-induced secondary particles encountered by the ISS while it passed through the South Atlantic Anomaly not present in the Antarctic balloon result.



Figure 5.4. Tracks in CR-39 PNTD exposed aboard the International Space Station.

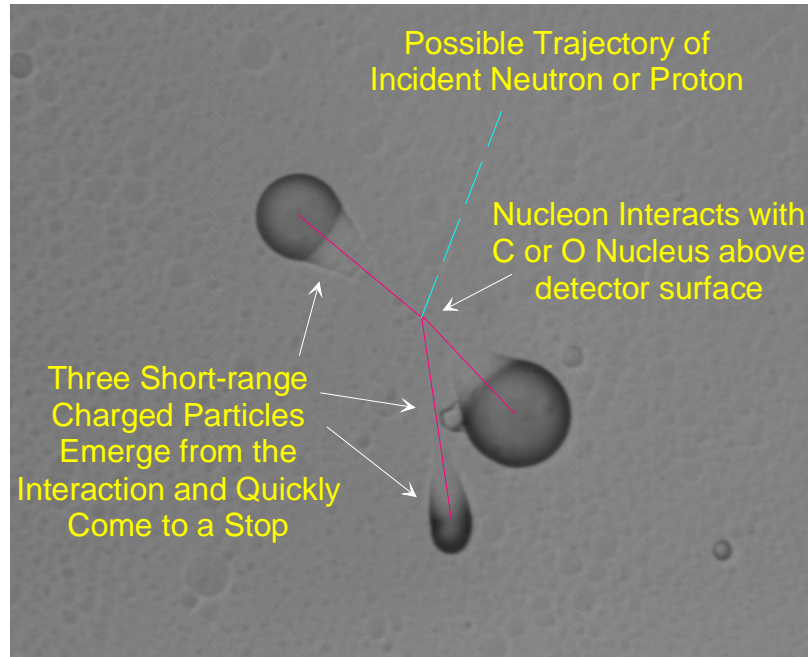


Figure 5.5. Tracks in CR-39 PNTD from secondary particles produced in a neutron- or proton-induced target fragmentation interaction. CR-39 PNTD was exposed aboard the NASA ER-2 high altitude research aircraft at ~70,000 ft (~20 km).

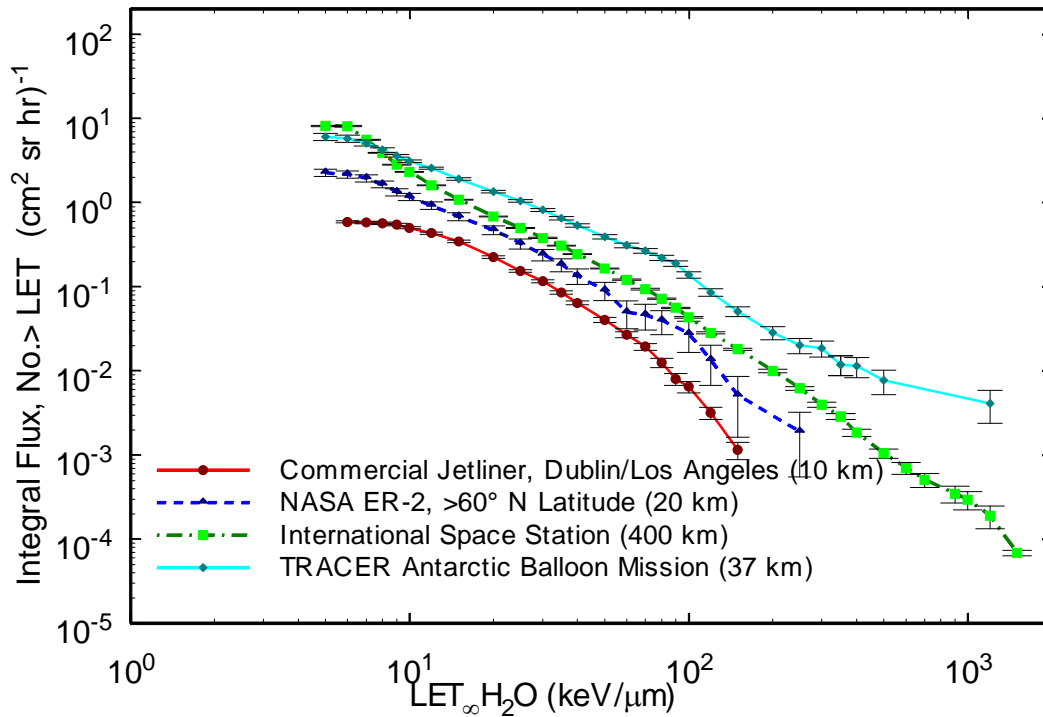


Figure 5.6. Integral LET Flux Spectra measured aboard a commercial jetliner flying between Dublin and Los Angeles, a NASA ER-2 high altitude research aircraft, the ISS, and the TRACER high altitude Antarctic research balloon.

Table 5.1. Average dose rate, average dose equivalent rate, and average quality factor from particles of $LET \geq 10 \text{ keV}/\mu\text{m}$ measured aboard a variety of spacecraft and aircraft.

Exposure	Dates	Duration (hr)	Average Altitude (km)	Average Dose Rate $\geq 10 \text{ keV}/\mu\text{m}$ ($\mu\text{Gy}/\text{hr}$)	Average Dose Eq. Rate $\geq 10 \text{ keV}/\mu\text{m}$ ($\mu\text{Sv}/\text{hr}$)	Average Quality Factor $\geq 10 \text{ keV}/\mu\text{m}$
Commercial 747 Dublin/LA route	8-10/2001	796	10	0.34 ± 0.01	3.11 ± 0.14	9.08 ± 0.49
NASA ER-2 $>60^\circ \text{ N. lat.}$	1-6/2000	46.5	20	0.52 ± 0.05	4.88 ± 0.86	9.33 ± 1.88
ISS Expedition 2	5-8/2001	2350	400	0.92 ± 0.03	9.38 ± 0.43	10.20 ± 0.35
TRACER Antarctic Balloon	12/2003	324	37	1.83 ± 0.07	22.34 ± 1.09	12.21 ± 0.76

6. Combined CR-39 PNTD/TLD Measurements

Numerous research groups have developed methods for obtaining total absorbed dose, total dose equivalent, and average quality factor using a combination of LET spectrum measured in CR-39 PNTD and absorbed dose measured in TLD [Doke et al., 1984; Benton et al., 2002]. Readout and analysis of the TLD and CR-39 PNTD components in each dosimeter are carried out separately. Absorbed dose and dose equivalent as functions of LET from particles of LET ≥ 10 keV/ μm are obtained from the LET spectrum measured in CR-39 PNTD as described in Section 5. Total absorbed dose is obtained from TLD as described in Section 4. Dose from particles of quality factor equal to 1, i.e. from particles of LET < 10 keV/ μm , is obtained with the aid of a TLD dose efficiency function. This is then combined with the dose and dose equivalent from particles of LET ≥ 10 keV/ μm measured in CR-39 PNTD to obtain total absorbed dose and dose equivalent. Table 6.1 shows the average total absorbed dose rates, average total dose equivalent rates, and average total quality factors (ratio of dose equivalent to absorbed dose) measured using the combination of LiF TLD and CR-39 PNTD aboard a variety of spacecraft and aircraft.

Table 6.1. Average total dose rate, average total dose equivalent rate, and average total quality factor from combined TLD/CR-39 PNTD measurements made aboard a variety of spacecraft and aircraft.

Exposure	Dates	Duration (hr)	Average Altitude (km)	Average Total Dose Rate ($\mu\text{Gy/hr}$)	Average Total Dose Eq. Rate ($\mu\text{Sv/hr}$)	Average Total Quality Factor
Commercial 747 Dublin/LA route	8-10/2001	796	10	2.52 ± 0.16	5.28 ± 0.40	2.10 ± 0.17
NASA ER-2 >60° N. lat.	1-6/2000	46.5	20	8.41 ± 1.29	12.77 ± 2.72	1.52 ± 0.36
STS-95 (28.5°)	11/1998	8.9	574	57.92 ± 4.58	201.25 ± 17.08	3.46 ± 0.35
ISS Expedition 2	5-8/2001	2350	400	10.36 ± 0.54	18.81 ± 1.11	1.82 ± 0.13
TRACER Antarctic Balloon	12/2003	324	37	5.47 ± 0.31	25.98 ± 1.68	4.75 ± 0.36

References

- [Apathy et al., 1999] Apathy, I., Deme, S., Bodnar, L., Csoke, A. and Hejja, I. (1999), "An on-board TLD system for dose monitoring on the International Space Station." *Rad. Prot. Dos.* **85** (1-4) 321-323.
- [Benton et al., 2000] Benton, E.R., Frank, A.L., and Benton, E.V. (2000) "TLD efficiency of ^7LiF for doses deposited by high-LET particles," *Rad. Meas.* **32** (3) pp.211-214.
- [Benton and Benton, 2001] Benton E. R. and Benton, E. V. (2001) "Space radiation in low-Earth orbit and beyond," *Nucl. Inst. & Meth. B*, **184** pp. 255-294.
- [Benton et al., 2001] Benton, E. R., Benton, E. V., and Frank, A. L. (2001) "Neutron dosimetry in low Earth orbit using passive dosimeters," *Rad. Meas.* **33** (3) 255-264.
- [Benton et al., 2002] Benton, E. R., Benton, E. V., and Frank, A. L. (2002) "Passive dosimetry aboard the Mir Orbital Station: internal measurements," *Rad. Meas.* **35** (5) 443-460.
- [Cartwright et al., 1978] Cartwright, B. G., Shirk, E. K., and Price, P. B. (1978) "A nuclear-track-recording polymer of unique sensitivity and resolution," *Nucl. Inst. & Meth.*, **153** 457-460.
- [Cassou & Benton, 1978] Cassou, R. M. and Benton, E. V. (1978) "Properties and applications of CR-39 polymeric nuclear track detector," *Nucl. Track Detec.*, **2** 173-179.
- [Doke et al., 1984] Doke, T., H. Tawara, T. Hayashi, H. Ichinose, K. Kuwahara, S. Nakamura, S. Orito and K. Ogura (1988). "CR-39 plastic for massive magnetic monopole search." *Nucl. Inst. & Meth. B*, **34** 81-88.
- [Henke & Benton, 1971] Henke, R.P. and Benton, E.V. (1971) "On geometry of tracks in dielectric nuclear track detectors," *Nucl. Inst. & Meth.*, **97** pp. 483-489.
- [ICRP, 1991] International Commission on Radiological Protection (1991), *1990 Recommendations of the International Commission on Radiological Protection*, ICRP Publication No. 60, Oxford.
- [NCRP, 2000] National Council on Radiation Protection (2000) *Radiation Protection Guidance for Activities in Low-Earth Orbit*, NCRP Report No. 132, Bethesda.
- [Reames, 1999] Reames, D. V. (1999), "Particle acceleration at the sun and in the heliosphere," *Space Sci. Rev.* **90**, 413-491.
- [Stassinopolus, 1988] Stassinopolus, E. G. (1988) "The Earth's trapped and transient space radiation environment", in *The Terrestrial Space Radiation Environment and its*

Biological Effects, P. D. McCormack, C. E. Swenberg, and H. Bucker eds. NATO ASI Series A: Life Sciences Vol. 154. Plenum Press, New York, pp. 5-36.